Template-assisted fabrication of tunable aspect ratio, biocompatible iron oxide pillar arrays

Ryan Chang Tseng[1], Ching-Wen Li[2], Gou-Jen Wang[1,2,3*]

[1]*Graduate Institute of Biomedical Engineering, National Chung-Hsing University, Taichung 402, Taiwan*
[2]*Department of Mechanical Engineering, National Chung-Hsing University, Taichung 402, Taiwan*
[3]*Tissue Engineering and Regenerative Medicine, National Chung-Hsing University, Taichung 402, Taiwan*

[*]Corresponding author

DOI: 10.5185/amlett.2018.1842
www.vbripress.com/aml

Abstract

The extensive use of iron oxide nanomaterials in biomedical applications has prompted the development of a novel substrate for evaluating cell behaviour. This study examines the fabrication of tuneable length iron oxide pillar arrays using the porous nanochannels of anodic aluminium oxide membranes, and evaluates the biocompatibility of the substrate. The electroformed iron pillars were found to conform to the template channels with slightly larger iron oxide pillar diameters, due to the presence of an oxide shell. The biocompatibility was then confirmed with WST-1 proliferation and viability assay of cultured KT98 murine neural/progenitor stem cells on the surface of the pillar array; with no significant difference observed between viable cells after seven days of culture on iron oxide pillars, flat iron oxide, and tissue culture polystyrene. The physical properties of the pillar arrays were linked to the adhesion and spreading of the cells, and found that cells cultured on the pillar arrays had reduced spreading in comparison to tissue culture polystyrene control. In addition, it was found that protein expression was unaffected by culture on iron oxide substrates. The results of this study indicate that iron oxide pillar arrays are suitable to extended cell studies.

Keywords: Anodic aluminum oxide, template, electrodeposition, pillar array, iron oxide.

Introduction

The microenvironment in which cells reside in vivo exhibits a complex array of signals which play an essential role in cellular processes. Cells are capable of sensing and responding to a plethora of signals, consisting of biochemical and biophysical cues, over a wide range of length scales **[1]**. Many of these cues are provided by the extracellular matrix (ECM), which acts as a cellular scaffold and is the primary component of tissues. The interaction and response of cells with ECM topographies are mediated through a phenomenon termed contact guidance, and is known to affect cellular behaviors such as adhesion, morphology, migration, and differentiation **[2-4]**. Another type of physical cue displayed by the ECM is mechanical stiffness through which a diverse set of cellular functions can be modulated **[5]**.

Cells have been found to be sensitive to nanoscale topography of the substrate and this sensitivity has been observed across a variety of cell types including fibroblasts, osteoblasts, endothelial, epithelial and smooth muscle cells **[6, 7]**. The effects of periodic surface nanofeatures on cell behavior have been examined by using nanoscale patterns such as columns, dots, pits, pores, gratings, and random surface roughness created by nanolithography and nanofabrication techniques **[8-13]**. Applications for controlling cell behavior with nanostructured and nanopatterned materials range from improving integration of titanium implants with bone, to developing polymer scaffolds that better mimic the extracellular matrix, to anti-fouling materials for preventing cell adhesion in biomedical implants **[14-16]**.

One class of nanostructures that has received attention is a surface covered with upright slender cylinders, variously referred to as nanoposts, -rods, -columns, and –wires. These structures have been investigated for their ability to modulate cell adhesion and affect proliferation and differentiation, such as silicon dioxide (SiO_2) based nanowires. A study by Kim and colleagues has shown that stem cells can survive for long periods of time on surfaces coated with SiO_2 nanowires **[7]**. Conversely, on comparatively denser nanowires, cell adhesion was decreased, suggesting their potential for anti-fouling surfaces **[6]**. In a similar study it was shown that cell proliferation in fibroblasts was greatly reduced on needle-like silicon nanoposts **[6]**. However, another study demonstrated that mesenchymal stem cells on silicon nanowires survived for days, and even differentiated despite being impaled on the nanowires **[7]**. Kim et al. revealed that although cell spreading of A549 human lung tumor cells decreased on nanopillars and wires, cell viability was still comparable to those on planar substrates **[17]**. Therefore, it is not clear if different cell types will exhibit reduced cell survival on structures such as nanowires or nanorods.

As such, the fundamental mechanism of how physical stimuli contributes to the regulation of cell behaviors has yet to be fully elucidated. By understanding the way in which cells interact with their environment, there is potential to control cell behavior through the fabrication of substrates with distinctive physical properties. In the pursuit of clarifying these interactions, nano- and microfabrication technologies have been utilized to construct substrates of differing topographies in an attempt to mimic the ECM and to study specific cell behaviors **[18]**. In addition, these techniques have allowed for the design of platforms crucial to studying cell biomechanics and its importance in tissue organization and development **[19, 20]**.

Template-based synthesis is one of these fabrication techniques utilized. It is an inexpensive and technologically simple approach for the fabrication of various nanoscale materials. It provides an alternative method that overcomes many drawbacks of lithographic techniques and exploits various template characteristics, such as the material, pattern, order and periodicity, and feature size. Templating methods employ a variety of porous membranes and films, such as porous aluminum oxide, for the synthesis of high density, ordered arrays of nanodots, -tubes, and –wires **[21]**. The nanostructures can be obtained via atomic layer deposition by filling the holes of the porous materials and can host a variety of materials, such as metals, semiconductors, and oxides to produce structures with high conformity **[22]**.

Anodized aluminum oxide (AAO) membranes with high aspect ratio nanoholes or –pores have been widely used as a template for electrodeposition of metal nanoarrays. The oxidized membranes are characterized by perpendicular pores that are normal to the film's surface with controllable pore diameters and interpore spacing. Arrays of metallic nanowires and nanorods are mainly synthesized by the deposition of materials into the nanochannels of anodic porous alumina, such as arrays of Ag, Au, Co, Cu, Ni, Pb, and Pd **[23-31]**.

Magnetic iron oxide materials have received considerable attention as they are inexpensive to produce, physically and chemically stable, biocompatible, and environmentally safe. Hence, the use of iron oxides as contrast agents for in vitro diagnostics, targeted drug delivery, magnetic resonance imaging, magnetic hyperthermia, thermoablation, bioseparation, and biosensing are commonly found in literature and clinical applications **[32-34]**. Many of the useful attributes of iron oxide depend on the preparation method for the nanomaterials. The fabrication process is the determining factor for size, shape, distribution, surface chemistry and, hence, the application.

The need for chemical stimuli for differentiating stem and progenitor cells in tissue engineering and regenerative medicine applications is essential for directing the cell into the correct lineage. Cells in their natural environment experience both chemical and physical stimuli, and both these stimulus sources have been shown to work together synergistically **[35, 36]**. Numerous studies have been conducted on chemical stimulus or a combination of chemical and physical stimuli, but few studies have focused purely on physical stimulus effects on primary cell processes, such as proliferation, differentiation, adhesion, migration and morphology. Thus, the purpose of this study was to fabricate a substrate that would permit the investigation of pure physical stimulus on cells by, first, observing their static response through evaluating morphological changes and comparing the level of protein expression to the control substrate.

Experimental

Iron oxide pillar array fabrication

AAO membranes were used as templates for growing iron oxide pillar arrays. To prepare the aluminum foils (99.9995% purity, 130 μm thick) for AAO fabrication, they were washed in sequence with acetone, ethanol and deionized water. The washed aluminum foil was then electropolished using perchloric acid ($HClO_4$) and anhydrous ethanol solution (C_2H_5OH) under a constant voltage. The anodizing process was then carried out in 0.3 M oxalic acid solution at 0°C. Porous aluminum oxide was formed after anodizing for two hours. The unreacted aluminum beneath the barrier-layer was removed with an aqueous copper chloride ($CuCl_2$) and hydrochloric acid (HCl) solution.

To produce AAO through-hole nanochannels the barrier-layer was etched by immersing in a 0.1 M sodium hydroxide (NaOH) solution for 20 min at room temperature.

A 20 nm-thick layer of gold (Au) was sputter-deposited on the barrier-layer side of the AAO to serve as the electrode. A nickel (Ni) layer (10 μm) was then electroplated onto the sputtered Au; to increase the mechanical strength of the substrate and to act as a support base for the pillars. The electroplating of Ni was carried out with bulk nickel as the anode and the AAO template as the cathode in an aqueous solution of nickel sulfamate ($Ni(NH_2SO_3 \cdot 4H_2O$) and nickel chloride ($NiCl_4 \cdot 7H_2O$).

The iron (Fe) pillars were then electroformed using a similar system for electroplating Ni, with bulk low-carbon steel as the anode and AAO template as the cathode in an aqueous solution of ferrous sulfate ($FeSO_4 \cdot 7H_2O$) and iron chloride tetrahydrate ($FeCl_2 \cdot 4H_2O$).

Finally, the alumina was etched using a 1 M NaOH solution to obtain the pillar array. The pillar array was then oxidized under atmospheric pressure and temperature.

The schematic for the fabrication of iron oxide pillar arrays is shown in **Fig. S1**.

Material characterization

A field-emission scanning electron microscope (FESEM, JEOL JSM-7401F) was used to examine the parameters of the AAO template and the iron oxide pillars. For cross-sectional examination of the AAO the samples were mechanically broken, and for the pillars the samples were mechanically cut. Atomic force microscopy (AFM,

Bruker Dimension Icon) was performed to examine the surface topography and roughness of the samples. The Young's elastic modulus of the pillar arrays were evaluated using a Berkovich tip nanoindenter (TriboLab, Hysitron) Raman spectroscopy (Nanofinder 30, Tokyo Instruments Inc.) and energy dispersive spectroscopy (EDS, JEOL JSM-7401F) analysis were performed to determine and confirm the presence of iron oxide. The measurements of pore diameter, pillar diameter and pillar length were performed with ImageJ software.

Cell seeding and culture

To examine the biocompatibility and effect of the length of the nanopillar arrays, KT98 murine neural stem/progenitor cells were used. All cell culturing products were purchased from Gibco™ by Life Technologies™. The cells were cultured in Ham's F-12 Nutrient Mixture, supplemented with 10% fetal bovine serum, and 1% antibiotic/antimycotic, in a humidified CO_2 incubator at 37°C.

Cells were initially cultured in T75 cell culture flasks (Corning Inc.) until 90% confluent, trypsinized and seeded onto the iron oxide pillars in a 24-well culture plate (Corning Inc.). The cells were then cultured on the pillars for 48 hours with well-plate cell culture serving as control.

Cell proliferation and viability

Cell proliferation and viability assay was conducted with water-soluble tetrazolium kit (WST-1, BioVision Inc.) over seven days. The initial seeded concentration of cells on the material was 0.1×10^4 cells/mL in a 24-well plate and the culture medium was refreshed every second day. On the seventh day, the culture medium was removed and the pillars were washed with phosphate-buffered saline (PBS). The PBS was then replaced with a 1:10 WST-1 reagent to culture medium solution and left to incubate for three hours. 100 µL of the working solution was then placed into a 96-well ELISA plate reader and measured at a wavelength of 405 nm with a reference wavelength of 595 nm.

Immunofluorescent staining

After 48 hours, the cultured cells were washed with PBS and chemically fixed in a 4% (w/v) paraformaldehyde in PBS for 15 min at room temperature and then washed with PBS. The cells were then permeabilized with 0.1% (v/v) Triton X-100 in PBS for 10 min and washed. Non-specific blocking of the cells was applied with 3% (v/v) goat serum albumin (Gibco™) for 60 min and washed. Primary antibody mouse anti-vinculin (Affymetrix) was then incubated at a concentration of 1:300 in 3% goat serum overnight at 4°C. The cells were then washed and goat anti-mouse IgG (H+L) secondary antibody AlexaFluor® 488 (Thermo Fisher Scientific) was incubated at a concentration of 1:500 with 3% goat serum at room temperature for 60 min. DAPI and AlexaFluor® Phalloidin 568 were then incubated at room temperature at a concentration of 300 nM and 3.3 nM in PBS for 10 and 20 min, respectively, then washed and stored in PBS. The cells were then imaged with fluorescence microscopy (Leica DMIL LED). All products were purchased from Sigma-Aldrich unless stated otherwise.

SDS-PAGE and Western blotting

Briefly, cells were seeded at a density of 0.5×10^4 cells per substrate in a 24-well culture plate and cultured in a humidified CO_2 incubator at 37°C. After 48 hours, the cells were trypsinized from the substrate, centrifuged, and the cell pellet resuspended with Pierce™ IP Lysis Buffer (Thermo Fisher Scientific) and incubated at room temperature for 30 min. The solution was then centrifuged to separate the cell debris from the protein solution. For SDS-PAGE, each well in the gel was loaded with a working solution consisting of 20 µg of the protein sample and 4X Laemmli sample buffer. Prior to loading, the proteins were denatured via heating, and then loaded into the gel along with a standard protein ladder marker. After electrophoresis, the proteins were transferred to a nitrocellulose membrane. The membrane was then blocked in 5% (w/v) non-fat milk in phosphate-buffered saline with Tween 20 (PBST) for 60 min and washed thrice with PBST before incubating primary antibodies (concentration of 1:1000 with PBS; antibody stock concentration of 1 mg/mL) at 4°C overnight. The primary antibodies used were: mouse anti-vinculin (Affymetrix); rabbit anti-β-tubulin III (Sigma-Aldrich); mouse anti-nestin (Invitrogen); and for loading control, mouse anti-actin (Sigma-Aldrich). Secondary antibodies were then incubated for 90 min; antibodies used were: goat anti-rabbit IgG (H+L) IRDye®800 conjugated and goat anti-mouse IgG (H+L) IRDye®800 conjugated (Rockland Immunochemicals). The membranes were then imaged with Li-Cor Odyssey Infrared Imaging System.

Statistical analysis

Statistical comparisons of the data were analyzed with one-way analysis of variance (ANOVA) combined with Tukey's test with OriginPro 9 (OriginLab®).

Results and discussion

Electroformed iron oxide pillar arrays

From images obtained through scanning electron microscopy (SEM), it was possible to determine the average pillar diameter of the electroformed iron oxide pillar arrays **(Fig. 1).** The average pillar diameter was measured and found to be 244.2 ± 25.4 nm, compared with AAO pore diameters of 230.7 ± 21.9 nm (Fig. S2). A difference between the average diameters can be observed, which is suggested to arise from the oxidation of iron after template removal; as iron oxide occupies more volume than metallic iron, the diameter of the pillar increases. The observed result suggests that the oxide layer is, on average, 7 nm thick. It also demonstrates that

template-based electroformation of iron pillars is a precise fabrication method, as no significant difference was found between the average pillar and pore diameters.

The density of the pillars was also measured from various SEM images of different length pillar arrays and it was found that there is an average of 7.0 ± 0.63 pillars per μm^2, in comparison the density of the AAO pores was 9.64 ± 0.43 per μm^2. This observed difference was attributed to unintentional removal of pillars during processing, and pores on the AAO membrane not fully forming through-hole channels.

of lower pillar stiffness, magnetism, and a reduction of surface energy, but was not observed in every sample.

The significance of being able to control the electroformed pillar length is that this fabrication method can be applied to a variety of potential applications that require different aspect ratio pillars. The results also demonstrate that AAO is a suitable template as the electroformed iron pillars conformed precisely to the AAO channels.

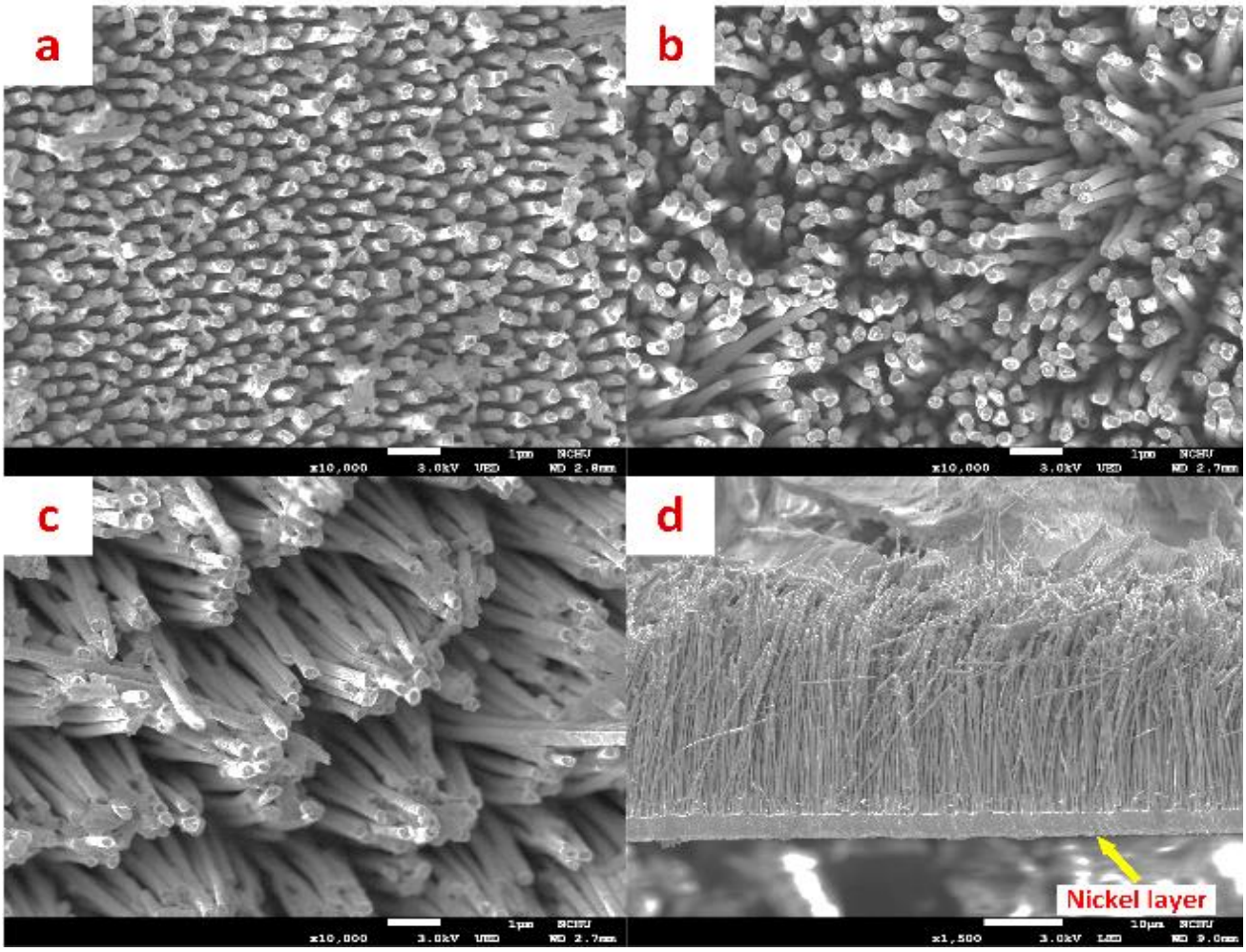

Fig. 1. SEM images of iron oxide pillars. Electrodeposition times of (a) 10 min, (b) 30 min, and (c) 60 min are shown, with (d) a cross-sectional image of 60 min electroformed iron pillars.

The length of the pillars was observed to increase with electrodeposition time, and accordingly, a linear trend can be observed **(Fig. 2).** The linearity implies that the length of the pillars can be precisely controlled by adjusting the electrodeposition time. The observed length of the pillars at 10, 30, and 60 min were 9.6 ± 1.3, 17.4 ± 1.3, and 27.8 ± 2.0 µm, respectively, with an average deposition rate of 0.36 µm per min. It can be seen that as the length of the pillars increased, the pillars were more susceptible to aggregation; this may have been caused due to a combination

It was necessary to confirm the oxidation of iron pillars as iron oxide has greater biocompatibility over metallic iron, hence energy dispersive spectroscopy (EDS) and Raman spectroscopy were performed. It is shown thatiron (Fe) and oxygen (O) are the predominant elemental species present from EDS. In addition, the Raman spectra of the iron oxide pillar arrays have peaks associated with known hematite (α-Fe_2O_3) samples, hence it can be confirmed that the iron pillars have indeed oxidized (Fig. S3).

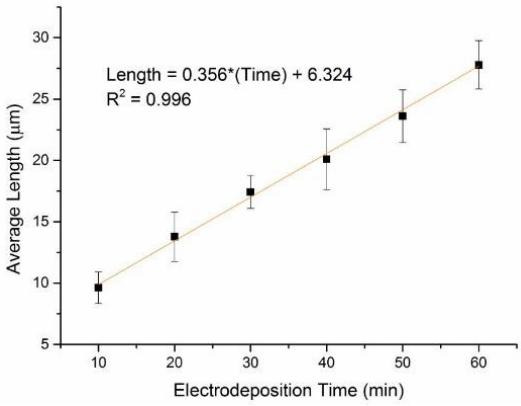

Fig. 2. Average pillar length at each electrodeposition time; the length increases at a linear rate with increased deposition time (n > 3).

The surface roughness and elastic modulus of the substrates were examined with atomic force microscopy and nanoindentation, respectively. The results of the scanned surfaces are summarized in **Table 1** (with representative images in Fig. S4). One-way analysis of variance, ANOVA, was performed on the roughness values (n = 3), and it was found that there were no significant differences at the 0.05 level. An insignificant result demonstrates that the electrodeposition of iron into the pores of the AAO are uniform, it also suggests that the effect of the surface roughness on subsequent cell experiments can be considered negligible; as the cells will, theoretically, all display the same characteristics if no other factors are considered.

Table 1. Comparisons between pillar length and surface roughness at different electrodeposition times.

Deposition Time (min)	Average Length (µm)	Average Roughness (nm)
Flat	-	49.6 ± 7.3
10	9.6 ± 1.3	66.3 ± 1.5
20	13.8 ± 2.0	56.0 ± 10.0
30	17.4 ± 1.3	60.1 ± 10.8
40	20.1 ± 2.5	46.6 ± 4.5
50	23.6 ± 2.1	51.8 ± 11.1
60	27.8 ± 2.0	65.3 ± 11.1

As the surface roughness was found to have insignificant differences, the other material property that would potentially affect cell culture is the stiffness of the substrate, hence nanoindentation was performed. In subsequent experiments the shortest length pillars (9.6 ± 1.3 µm), longest length pillars (27.8 ± 2 µm), and flat iron oxide were used; it was proposed that the selected pillar arrays would display the greatest difference in elastic modulus with the flat surface serving as a control for iron oxide substrates. It should be noted that the shortest pillar arrays will be denoted as Substrate 1 (S1), and the longest pillars denoted as Substrate 2 (S2), henceforth. Supplementary Fig. S5 illustrates the difference in elastic modulus of the different substrates; flat (6.3 ± 0.4 GPa), S1 (2.1 ± 0.2 GPa), S2 (1.3 ± 0.4 GPa). It was found that each group was significantly different from each other at the 0.05 level, hence it was suggested that any differences in subsequent experimentation may be attributed to the variation in stiffness of the samples.

Cell spreading and morphology

Through fluorescent staining of the cells after 48 hours of culture it was possible to determine cell spread through measuring and evaluating the adhesion plaques. Shown in **Fig. 3**, the cell morphologies of TCPS appear to be more spread; with a greater number of neurite outgrowth, cell cultures on iron oxide pillar arrays seemly more similar to each other, and flat iron oxide substrate culture more closely resembling TCPS, but with greater filopodia occurrence (**Fig. 3(d)).** The measured areas are shown in **Fig. 4** (and Fig. S6), with significant differences found between TCPS – S1 and TCPS – S2, as well as between S1 – flat iron oxide. The differences between TCPS and the iron oxide pillar arrays may be attributed to the pre-treated and coated TCPS, which allows for greater adhesion and spreading. The pillar features may also affect integrin clustering, which may have resulted in the observed lower cell spreading and adhesion area.

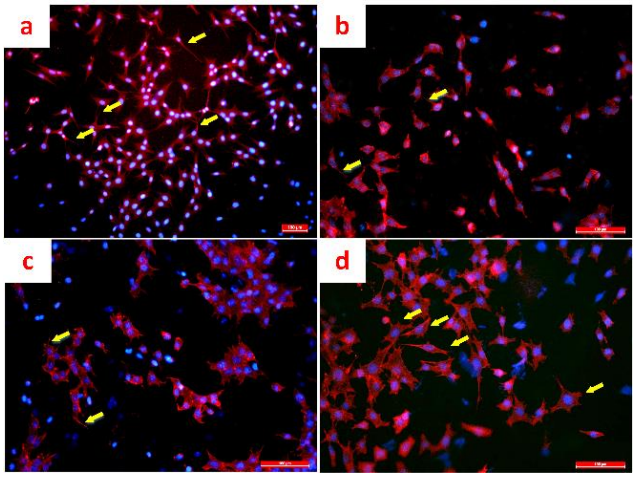

Fig. 3. Fluorescent images of cells cultured on (a) TCPS; (b) substrate S1; (c) substrate S2; and (d) flat iron oxide. Cells were stained with cytoskeletal stain, Phalloidin (red), and the nuclei were counterstained with DAPI (blue). The arrows indicate neurite outgrowths. Scale bars are 100 µm.

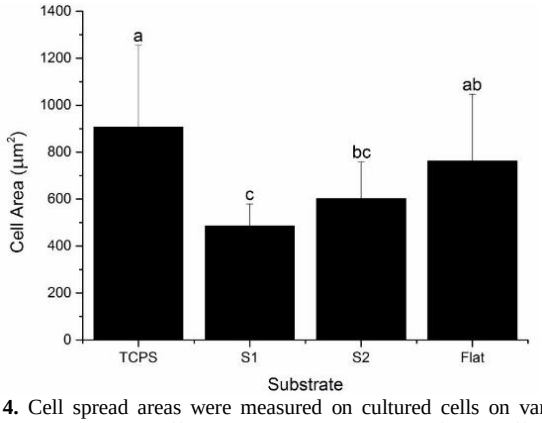

Fig. 4. Cell spread areas were measured on cultured cells on various substrates (n > 15). Different letters indicate a significant difference between groups at the 0.05 level.

Biocompatibility of iron oxide pillar arrays

The biocompatibility of the fabricated iron oxide pillars were evaluated with KT98 neural stem/progenitor cells and WST-1 assay kit, where tetrazolium salt WST-1 is cleaved to form insoluble formazan by mitochondrial dehydrogenases. The formazan dye produced by viable cells is then excited with 440 nm light and the absorbance measured to quantify the amount of viable cells. It was observed that there appeared to be no significant differences in the viability of cells across the sample groups after seven days (including TCPS); although there were observed discrepancies between groups for the average number of viable cells **(Fig. 5)**. The results indicate that the long term survival of the cells is not adversely affected by culture on iron oxide substrates.

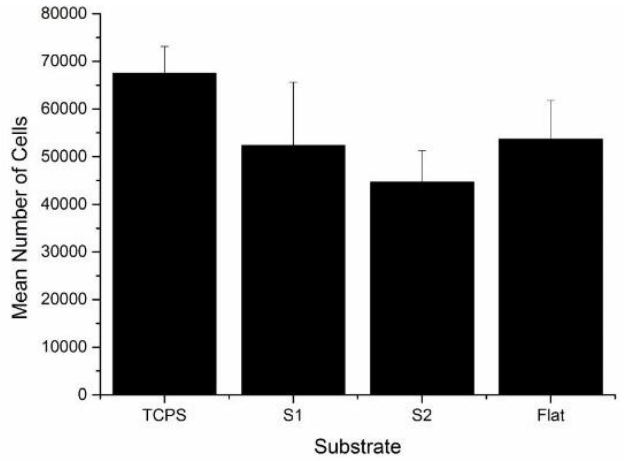

Fig. 5. Average number of viable cells cultured on substrates after seven days. (n > 3). No significant differences were found between groups at the 0.05 level.

Protein expression levels

The level of protein expression is another indicator that the cells function normally on the culture substrate, hence, in this study, β–tubulin III, vinculin, and nestin were evaluated and their protein expressions on different culture substrates compared.

The first protein, β–tubulin III, is an integral component of microtubules and is found in the brain and dorsal root ganglia, mainly localized to neurons of the central and peripheral nervous system. This protein is widely regarded as a neuronal marker in development neurobiology and stem cell research, and contributes to microtubule formation in neuronal cell bodies and axons, as well as roles in axonal transport, neuronal cell proliferation, and differentiation **[37]**. The second protein examined was vinculin, which is a membrane-cytoskeletal protein in focal adhesion plaques involved in cell-matrix and cell-cell adhesion. This protein is involved in the linkage of integrin adhesion complexes to the actin cytoskeleton by anchoring actin filaments to the membrane, hence, it is important for cell adhesion and spreading **[38]**. The third protein, nestin, is an intermediate filament protein that is expressed chiefly in nerve cells during the early stages of development in the central and peripheral nervous system. Differentiation of neural stem/progenitor cells downregulates its expression and is replaced by lineage-specific intermediate filament proteins **[39]**. **Fig. 6** illustrates the expression levels of each protein within cell populations cultured on each substrate; from this it can be seen that there are no significant differences in the expression levels of these proteins across the substrates. This demonstrates that these culture substrates do not adversely affect protein synthesis, particularly those involved with microtubule formation, focal adhesions, and multipotency of KT98 murine neural stem/progenitor cells.

While iron oxide nanoparticles have been used extensively in biomedicine for applications in diagnostics and therapy, this study proposes an alternative application in cellular engineering. The purpose of this study was to develop iron oxide pillar arrays with inherent magnetic properties able to be physically manipulated to stimulate cell cultures by, firstly, examining the biocompatibility and effect of static substrates on cell cultures without actuation. KT98 neural stem/progenitor cells were used in this study due to their multipotent capabilities, as demonstrated by Hsu et al **[40]**. The evaluation of KT98 cells' response to the fabricated iron oxide pillars determines the suitability of the material-cell combination for future studies on differentiation.

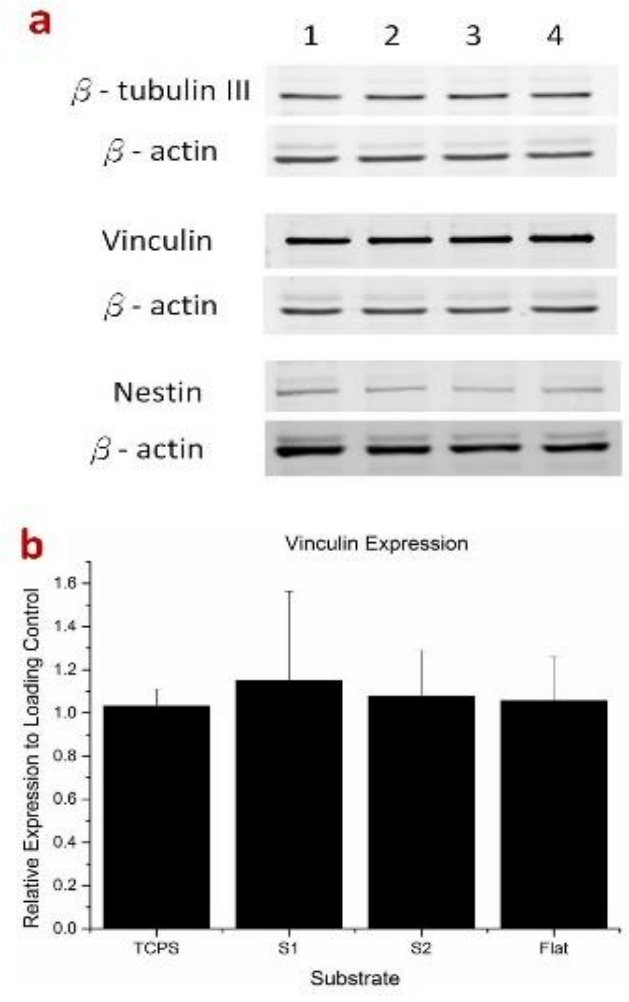

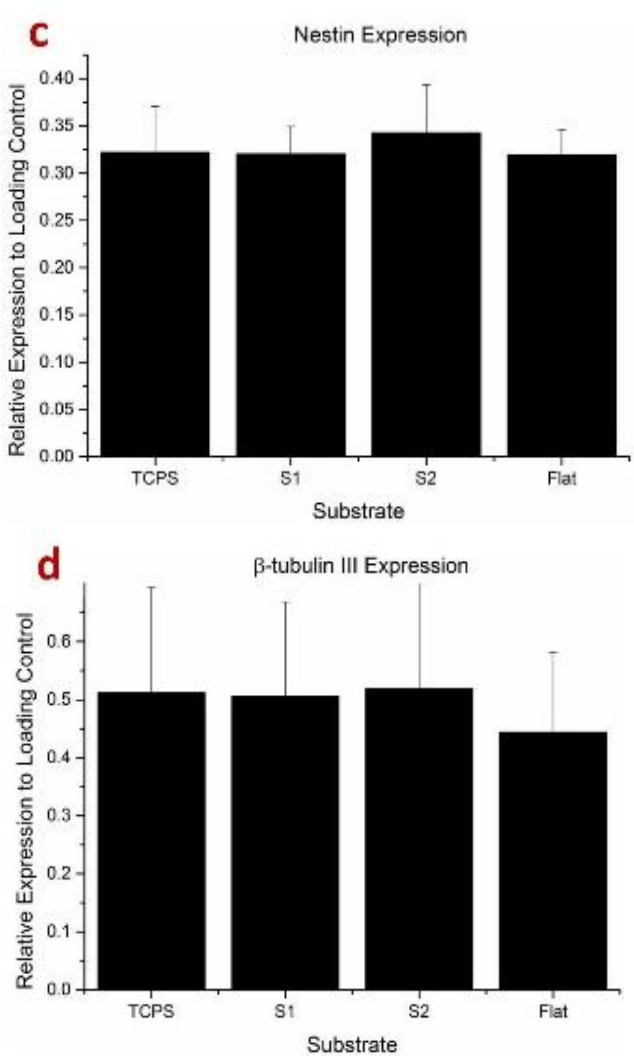

Fig. 6. SDS-PAGE and Western blotting of the protein expressions of KT98 cells culturedon different substrates (n = 4). (a) Western blotted membrane revealing protein bands of whole cell lysate from 1: TCPS; 2: S1 substrate; 3: S2 substrate; and 4: flat iron oxide. β-actin was used as loading control for all experiments.

From the above results, it can be seen that although there are slight differences in the culture of KT98 cells on the various iron oxide substrates, they do not significantly affect the growth, proliferation, and survivability of the cells in vitro.

In a study by Qi et al. it was found that silicon nanowire arrays restricted the spreading of cells, but increased cell adhesion **[41]**. Briefly, it was proposed that non-flat nanofeatures stimulate cells to extend more filopodia to form adhesion points with the substrate by reaching out to as many nanowires as possible. However, large spatial intervals between the nanowires made it difficult for the cells to reach the nanostructures that were too far from their initial point of contact, hence, cell spreading was restricted locally. In a similar study by Kim et al. on nanopillars and –wires, it was demonstrated that greater cell spreading did not necessarily correlate to increased cell viability; which the results of this study is in agreement **[17]**. In regards to this study, it may be entirely probable that, although S1 substrate demonstrated reduced cell spreading, cell adhesion was enhanced. It is seen that the cell areas on the S1 substrate are lower than that of the others, with significant differences with TCPS and flat iron oxide, but not with S2. It is possible that the reduction in cell adhesion area induces apoptosis through signaling pathways associated with focal adhesions **[42]**. It has been reported that the activation of focal adhesion kinase is directly involved in the promotion of cyclin and cyclin-dependent kinase synthesis, which in turn govern the entry of cells into the various stages of the cell cycle; hence a reduced adhesion will directly affect cell proliferation. In addition, the same reasoning can be applied to the S2 substrate, which demonstrates significant differences in cell adhesion areas with TCPS and flat substrates, but not with S1. It has also been reported that longer surface features reduce the proliferation rate of cells, which can be seen in the results of the viability assay **[43]**. This result potentially changes current perspectives that greater cell spreading enhances proliferation and survival, and requires further investigation into mechanisms and pathways that link adhesion, spreading and proliferation on nanowire and –pillar arrays.

In terms of protein expression, the results imply that culturing on iron oxide pillar arrays do not affect protein synthesis; as no differences were detected between protein expressions of β-tubulin III, vinculin, and nestin. These proteins were tested due to their direct and indirect involvement with many essential cellular processes, and no difference in their expression suggest that the cells are functioning normally. In a similar study on semiconductor nanowire arrays, it was found that the material and nanowire topography did not inhibit protein expression and was not harmful to cell function **[44]**. Although, the study utilized low density nanowire array, whereas in this study cells lay on top of a dense pillar array, it can be confirmed that protein expression is not adversely affected by culture on pillar features. This study is also concordant with reports that iron oxide materials present insignificant cytotoxic effects in vitro and in vivo **[45]**.

Reports have shown that the mechanical properties of the culture substrate can alter ECM assembly, cell spreading, and motility. For example, it has been shown that neural stem/progenitor cells prefer soft substrates, with stiffness in the range of 1 to 10 kPa **[46]**. In this study, it is possible that the cells were unable to perceive distinct differences between iron oxide pillar arrays due to substrates being overly stiff; with substrate stiffness in this study shown to be greater than 1 GPa. Hence, no significant differences were observed in the cell behavior results between long and short iron oxide pillars. Another possible issue is that the pillar arrays used in this study were too dense, increasing the interference of adjacent pillars that prevented cells from pulling on them. In addition, an insignificant difference in the surface roughness could have also contributed to the observed results. It is proposed that in future studies the density can be altered, via template modification, to increase spatial intervals to better evaluate cell response.

Conclusion

Iron oxide pillar arrays present an alternative means to evaluate cell response and can be utilized in a variety of settings due to the ease of tuning the pillar lengths and densities (dependent on the template dimensions). This study has demonstrated the ease of fabrication of tunable aspect ratio iron oxide pillars with a focus on applications in biomedicine and potential investigations into the mechanical stimulus on stem/progenitor cells. It has been demonstrated that the pillar arrays are biocompatible with no significant differences in the number of viable cells compared with TCPS and flat substrates. The protein expression of the cells cultured on the pillar arrays also displayed no differences with control groups, indicating that the combination of topographical features and iron oxide do not affect protein synthesis. The fabricated substrate may also be functionalized, similar to iron oxide nanoparticles, and in combination with high aspect ratio and enhanced surface areas will further broaden the range of applications not only in biomedicine, but catalysis and biosensing.

Acknowledgements

The authors would like to offer their thanks to the Ministry of Science and Technology of Taiwan under grant number MOST-103-2221-E-005-046-MY2 for their financial support of this research. The authors also would express their sincere appreciation to Professor Ing-Ming Chiu of National Health Research Institutes, Taiwan for kindly providing KT98 cells.

Author's contributions

GJW and CWL conceived the plan; RCT performed the experiments and data analysis; All author's contributed to the writing of this paper. Authors have no competing financial interests.

Supporting information

Supporting informations are available from VBRI Press.

References

1. Guck, J.; Lautenschlager, F.; Paschke, S.; Beil, M.; Integrative Biology, **2010,** 2, 575. **DOI**: 10.1039/c0ib00050g
2. Dunn, G. A.; Brown, A. F.; Journal of Cell Science, **1986,** 83, 313. Retrieved: http://jcs.biologists.org/content/83/1/313.long
3. Dent, E. W.; Gertler, F. B.; Neuron, **2003,** 40, 209. **DOI**: 10.1016/S0896-6273(03)00633-0
4. Haga, H.; Irahara, C.; Kobayashi, R.; Nakagaki, T.; Kawabata, K.; Biophysical Journal, **2005,** 88, 2250. **DOI**: 10.1529/biophysj.104.047654
5. Eyckmans, J.; Boudou, T.; Yu, X.; Chen, Christopher S.; Developmental Cell, **2011,** 21, 35. **DOI**: 10.1016/j.devcel.2011.06.015
6. Choi, C. H.; Hagvall, S. H.; Wu, B. M.; Dunn, J. C.; Beygui, R. E.; Kim, C. J.; Biomaterials, **2007,** 28, 1672. **DOI**: 10.1016/j.biomaterials.2006.11.031
7. Kim, W.; Ng, J. K.; Kunitake, M. E.; Conklin, B. R.; Yang, P.; Journal of the American Chemical Society, **2007,** 129, 7228. **DOI**: 10.1021/ja071456k
8. Yim, E. K. F.; Reano, R. M.; Pang, S. W.; Yee, A. F.; Chen, C. S.; Leong, K. W.; Biomaterials, **2005,** 26, 5405. **DOI**: 10.1016/j.biomaterials.2005.01.058
9. Turner, S.; Kam, L.; Isaacson, M.; Craighead, H. G.; Shain, W.; Turner, J.; Journal of Vacuum Science & Technology B: Microelectronics and Nanometer Structures Processing, Measurement, and Phenomena, **1997,** 15, 2848. **DOI**: 10.1116/1.589742
10. Wood, M. A.; Wilkinson, C. D.; Curtis, A. S.; IEEE transactions on nanobioscience, **2006,** 5, 20. **DOI**: 10.1109/TNB.2005.864015
11. Dalby, M. J.; Gadegaard, N.; Riehle, M. O.; Wilkinson, C. D. W.; Curtis, A. S. G.; The International Journal of Biochemistry & Cell Biology, **2004,** 36, 2005. **DOI**: 10.1016/j.biocel.2004.03.001
12. Ingham, C. J.; ter Maat, J.; de Vos, W. M.; Biotechnology Advances, **2012,** 30, 1089. **DOI**: 10.1016/j.biotechadv.2011.08.005
13. Miller, D. C.; Thapa, A.; Haberstroh, K. M.; Webster, T. J.; Biomaterials, **2004,** 25, 5. **DOI**: 10.1016/S0142-9612(03)00471-X
14. Olivares-Navarrete, R.; Hyzy, S. L.; Haithcock, D. A.; Cundiff, C. A.; Schwartz, Z.; Boyan, B. D.; Bone, **2015,** 73, 208. **DOI**: 10.1016/j.bone.2014.12.057
15. Smith, J. O.; Tayton, E. R.; Khan, F.; Aarvold, A.; Cook, R. B.; Goodship, A.; Bradley, M.; Oreffo, R. O. C.; Journal of Tissue Engineering and Regenerative Medicine, **2017,** 11, 1065. **DOI**: 10.1002/term.2007
16. Lee, J.; Chu, B. H.; Chen, K. H.; Ren, F.; Lele, T. P.; Biomaterials, **2009,** 30, 4488. **DOI**: 10.1016/j.biomaterials.2009.05.028
17. Kim, D. J.; Seol, J. K.; Lee, G.; Kim, G. S.; Lee, S. K.; Nanotechnology, **2012,** 23, 395102. **DOI**: 10.1088/0957-4484/23/39/395102
18. Park, T. H.; Shuler, M. L.; Biotechnology Progress, **2003,** 19, 243. **DOI**: 10.1021/bp020143k
19. Bettinger, C. J.; Langer, R.; Borenstein, J. T.; Angewandte Chemie (International ed. in English), **2009,** 48, 5406. **DOI**: 10.1002/anie.200805179
20. Nikkhah, M.; Edalat, F.; Manoucheri, S.; Khademhosseini, A.; Biomaterials, **2012,** 33, 5230. **DOI**: 10.1016/j.biomaterials.2012.03.079
21. Martín, J. I.; Nogués, J.; Liu, K.; Vicent, J. L.; Schuller, I. K.; Journal of Magnetism and Magnetic Materials, **2003,** 256, 449. **DOI**: 10.1016/S0304-8853(02)00898-3
22. Sulka, G. D.; Nanostructured Materials in Electrochemistry, Wiley-VCH Verlag GmbH & Co. KGaA: 2008. **DOI**: 10.1002/9783527621507
23. Xu, X. J.; Fei, G. T.; Wang, X. W.; Jin, Z.; Yu, W. H.; Zhang, L. D.; Materials Letters **2007,** 61, 19. **DOI**: 10.1016/j.matlet.2006.03.143
24. Sander, M. S.; Tan, L. S.; Advanced Functional Materials, **2003,** 13, 393. **DOI**: 10.1002/adfm.200304290
25. Evans, P.; Hendren, W. R.; Atkinson, R.; Wurtz, G. A.; Dickson, W.; Zayats, A. V.; Pollard, R. J.; Nanotechnology, **2006,** 17, 5746. **DOI**: 10.1088/0957-4484/17/23/006
26. Nielsch, K.; Wehrspohn, R. B.; Barthel, J.; Kirschner, J.; Fischer, S. F.; Kronmüller, H.; Schweinböck, T.; Weiss, D.; Gösele, U.; Journal of Magnetism and Magnetic Materials, **2002,** 249, 234. **DOI**: 10.1016/S0304-8853(02)00536-X
27. Chaure, N. B.; Stamenov, P.; Rhen, F. M. F.; Coey, J. M. D.; Journal of Magnetism and Magnetic Materials, **2005,** 290, 1210. **DOI**: 10.1016/j.jmmm.2004.11.387
28. Pang, Y. T.; Meng, G. W.; Fang, Q.; Zhang, L. D.; Nanotechnology, **2003,** 14, 20. **DOI**: 10.1088/0957-4484/14/1/305
29. Pang, Y. T.; Meng, G. W.; Zhang, Y.; Fang, Q.; Zhang, L. D.; Applied Physics A, **2003,** 76, 533. **DOI**: 10.1007/s00339-002-1483-8
30. Pang, Y. T.; Meng, G. W.; Zhang, L. D.; Shan, W. J.; Gao, X. Y.; Zhao, A. W.; Mao, Y. Q.; Journal of Physics: Condensed Matter, **2002,** 14, 11729. **DOI**: 10.1088/0953-8984/14/45/314
31. Kim, K.; Kim, M.; Cho, S. M.; Materials Chemistry and Physics, **2006,** 96, 278. **DOI**: 10.1016/j.matchemphys.2005.07.013
32. Teja, A. S.; Koh, P.-Y.; Progress in Crystal Growth and Characterization of Materials, **2009,** 55, 22. **DOI**: 10.1016/j.pcrysgrow.2008.08.003
33. Lee, N.; Hyeon, T.; Chemical Society Reviews, **2012,** 41, 2575. **DOI**: 10.1039/C1CS15248C

34. Laurent, S.; Dutz, S.; Häfeli, U. O.; Mahmoudi, M.; Advances in Colloid and Interface Science, **2011,** 166, 8.
DOI: 10.1016/j.cis.2011.04.003
35. Ge, D.; Liu, X.; Li, L.; Wu, J.; Tu, Q.; Shi, Y.; Chen, H.; Biochemical and Biophysical Research Communications, **2009,** 381, 317.
DOI: 10.1016/j.bbrc.2009.01.173
36. Abdellatef, S. A.; Ohi, A.; Nabatame, T.; Taniguchi, A.; International Journal of Molecular Sciences, **2014,** 15, 4299.
DOI: 10.3390/ijms15034299
37. Katsetos, C. D.; Legido, A.; Perentes, E.; Mörk, S. J.; Journal of Child Neurology, **2003,** 18, 851.
DOI: 10.1177/088307380301801205
38. Humphries, J. D.; Wang, P.; Streuli, C.; Geiger, B.; Humphries, M. J.; Ballestrem, C.; J. Cell. Biol., **2007,** 179, 1043.
DOI: 10.1083/jcb.200703036
39. Park, D.; Xiang, A. P.; Mao, F. F.; Zhang, L.; Di, C.-G.; Liu, X.-M.; Shao, Y.; Ma, B.-F.; Lee, J.-H.; Ha, K.-S.; Walton, N.; Lahn, B. T.; Stem Cells, **2010,** 28, 2162.
DOI: 10.1002/stem.541
40. Hsu, Y.-C.; Lee, D.-C.; Chen, S.-L.; Liao, W.-C.; Lin, J.-W.; Chiu, W.-T.; Chiu, I.-M.; Developmental Dynamics, **2009,** 238, 302.
DOI: 10.1002/dvdy.21753
41. Qi, S.; Yi, C.; Ji, S.; Fong, C.-C.; Yang, M.; ACS Applied Materials & Interfaces, **2009,** 1, 30.
DOI: 10.1021/am800027d
42. Gérard, C.; Goldbeter, A.; Interface Focus, **2014,** 4, 20130075.
DOI: 10.1098/rsfs.2013.0075
43. Persson, H.; Køber, C.; Mølhave, K.; Samuelson, L.; Tegenfeldt, J. O.; Oredsson, S.; Prinz, C. N.; Small, **2013,** 9, 4006.
DOI: 10.1002/smll.201300644
44. Berthing, T.; Bonde, S.; Sørensen, C. B.; Utko, P.; Nygård, J.; Martinez, K. L.; Small, **2011,** 7, 640-647.
DOI: 10.1002/smll.201001642
45. Huang, D.-M.; Hsiao, J.-K.; Chen, Y.-C.; Chien, L.-Y.; Yao, M.; Chen, Y.-K.; Ko, B.-S.; Hsu, S.-C.; Tai, L.-A.; Cheng, H.-Y.; Wang, S.-W.; Yang, C.-S.; Chen, Y.-C.; Biomaterials, **2009,** 30, 3645.
DOI: 10.1016/j.biomaterials.2009.03.032
46. Leipzig, N. D.; Shoichet, M. S.; Biomaterials, **2009,** 30, 6867.
DOI: 10.1016/j.biomaterials.2009.09.002

